Characterization of a submillimeter high-angular-resolution camera with a monolithic silicon bolometer array for the Caltech Submillimeter Observatory

Ning Wang, T. R. Hunter, D. J. Benford, E. Serabyn, D. C. Lis, T. G. Phillips, S. H. Moseley, K. Boyce, A. Szymkowiak, C. Allen, B. Mott, and J. Gygax

We constructed a 24-pixel bolometer camera operating in the 350- and 450-μm atmospheric windows for the Caltech Submillimeter Observatory (CSO). This instrument uses a monolithic silicon bolometer array that is cooled to approximately 300 mK by a single-shot ^{3}He refrigerator. First-stage amplification is provided by field-effect transistors at approximately 130 K. The sky is imaged onto the bolometer array by means of several mirrors outside the Dewar and a cold off-axis elliptical mirror inside the cryostat. The beam is defined by cold aperture and field stops, which eliminates the need for any condensing horns. We describe the instrument, present measurements of the physical properties of the bolometer array, describe the performance of the electronics and the data-acquisition system, and demonstrate the sensitivity of the instrument operating at the observatory. Approximate detector noise at 350 μm is 5×10^{-15} W/$\sqrt{\text{Hz}}$, referenced to the entrance of the Dewar, and the CSO system noise-equivalent flux density is approximately 4 Jy/$\sqrt{\text{Hz}}$. These values are within a factor of 2.5 of the background limit.

Key words: Submillimeter camera, bolometer array, monolithic silicon bolometer.

1. Introduction

To understand the process of star formation and the evolution of galaxies, it is necessary to understand the physical and chemical properties of the interstellar medium, which sometimes requires continuum observations of dust emission at submillimeter wavelengths over a sizable area. These observations call for the construction of a submillimeter continuum camera, which has the obvious advantage of increasing the efficiency of the telescope compared with the single-pixel bolometer currently available at the Caltech Submillimeter Observatory (CSO); it can also allow better reduction of sky noise.

We constructed a continuum camera for the CSO that operates in the 350- and 450-μm atmospheric windows. It uses a monolithic linear silicon bolometer array fabricated by the microelectronics laboratory at the Goddard Space Flight Center (GSFC). The array has 24 pixels, the pixel-to-pixel spacing is 1 mm, and the gaps are approximately 15 μm. No Winston cones[1] are used in the camera. Instead, we use off-axis elliptical mirrors to reimage the sky onto the bolometer array, and we use aperture and field stops to define the beam. We designed the optics so that each pixel subtends 5 arc sec × 10 arc sec on the sky, so that at a wavelength of 400 μm the pixels Nyquist sample the diffraction pattern along the array (the CSO has a 10.4-m-diameter telescope, so the diffraction beam width is approximately 8 arcsec at 400 μm).

As with a conventional bolometric instrument, cooled field-effect transistors (FET's) are used in the first stage of amplification, followed by room-temperature amplifiers. Signals from the output of the room-temperature amplifiers are digitized at 1

N. Wang, T. R. Hunter, D. J. Benford, E. Serabyn, D. C. Lis, and T. G. Phillips are with the California Institute of Technology, M/S 320-47, Pasadena, California 91125. S. H. Moseley, K. Boyce, A. Szymkowiak, C. Allen, and B. Mott are with the Goddard Space Flight Center, National Aeronautics and Space Administration, Greenbelt, Maryland 20771. J. Gygax is with Swales and Associates, Inc., 5050 Powder Mill Road, Beltsville, Maryland 20705.

Received 16 January 1996; revised manuscript received 6 May 1996.

0003-6935/96/346629-12$10.00/0

kHz. To ensure that all the signals are digitized simultaneously, each pixel has its own analog-to-digital converter (ADC), which was designed by R. G. Baker, W. Folz, and S. H. Moseley at the GSFC, NASA. A special digital signal processing (DSP) board, designed by A. Szymkowiak, K. Boyce, R. G. Baker, S. H. Moseley, W. Folz, and R. F. Loewenstein, performs the digital lock-in measurement. To isolate digital noise from the computer, fiber-optic cables are used to transmit the digital signal from the ADC's to the DSP board. The DSP board is situated inside a back-end computer assigned to the camera. Communication between the back-end computer, the telescope control computer, and the system control computer to monitor the timing of the idle and acquire states of the telescope is undertaken by way of Ethernet.

We fully tested the camera in the laboratory and successfully operated the camera on the telescope. In the 450-μm window, the optical responsivity is approximately 9×10^6 V/W, the total quantum efficiency is approximately 9%, and the optical noise-equivalent power (NEP) is approximately 6×10^{-15} W/$\sqrt{\text{Hz}}$. In the 350-μm window, the optical responsivity is approximately 1×10^7 V/W, the total quantum efficiency is approximately 10%, the optical NEP is approximately 5×10^{-15} W/$\sqrt{\text{Hz}}$, and the noise-equivalent flux density (NEFD) is approximately 4 Jy/$\sqrt{\text{Hz}}$. The camera is optically diffraction limited.

In this paper, we describe the configuration of the cryostat, show the schematics of the instrument, present the physical properties of the bolometer array, discuss briefly the electronics and the data-acquisition system, and summarize the important characteristics of the camera.

2. Cryogenics and Optics Description

A bolometer camera is a complex system involving cryogenics, optics, detector physics, electronics, and data-acquisition hardware and software. In this section, we describe the cryogenic and optical components of the bolometer camera.

A. Cryogenics

Figure 1 shows a schematic diagram of the CSO submillimeter camera. The cryostat, with a liquid-nitrogen and liquid-helium bath, is a single-shot ^{3}He refrigerator.[2] The liquid-nitrogen bath has a volume of approximately 5 L, and the liquid-helium bath has a volume of approximately 4 L. Under normal operation, the ^{4}He bath is pumped with a mechanical pump and operates at approximately 1.5 K. The hold time is approximately 18 h on the telescope, which limits the continuous operating time of the instrument. There are 3.2 L (STP) of ^{3}He gas, which is stored in a tank that is mounted on the cryostat and cycled during each cool down. The ^{3}He gas is condensed into a pot, which is suspended by Kevlar threads from the ^{4}He bath. The ^{3}He pot is pumped by a charcoal pump thermally linked to the ^{4}He bath. The base temperature of the ^{3}He pot is approximately

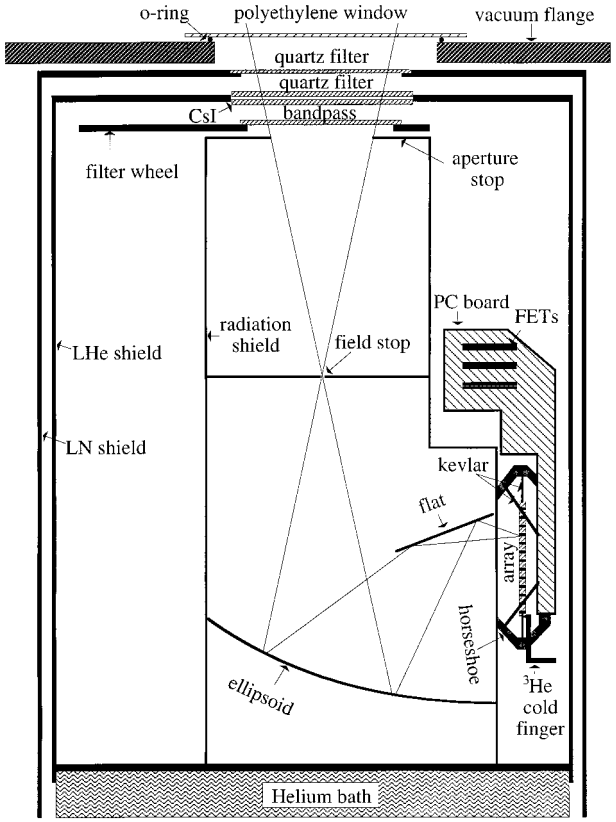

Fig. 1. Schematic diagram of the CSO submillimeter camera. PC, printed circuit.

295 mK. A mechanically driven heat switch is used to control the thermal link between the ^{3}He pot and the ^{4}He bath, and a second switch is used between the charcoal pump and the ^{4}He bath. Both switches are operated from outside the cryostat. Careful baffling around the ^{3}He pot is required to ensure that little 300-K background radiation from the heat-switch drivers reaches the bolometer array. Even though this type of background radiation causes little excess power load on the bolometer, it can be an additional source of noise, limiting the NEP of the bolometer array. We discuss this in more detail later in the paper.

B. Optics Overview

Most recent bolometer systems at $\lambda > 200$ μm rely on Winston cones. However, one of the unique features of this instrument is the lack of beam-defining cones, which allows us to use closely packed bolometer pixels to form an array in such a way that Nyquist sampling of the diffraction pattern can be achieved at the wavelengths of interest. We use mirrors to focus the light onto the detector pixels and an aperture stop and a field stop to define the primary illumination and the field of view.

Figure 2 is a diagram of the camera's optics. The telescope's Cassegrain focus is reimaged by an off-axis elliptical mirror outside the cryostat,[3,4] and the image of the primary is placed below the lid of the helium shield inside the cryostat. To form this im-

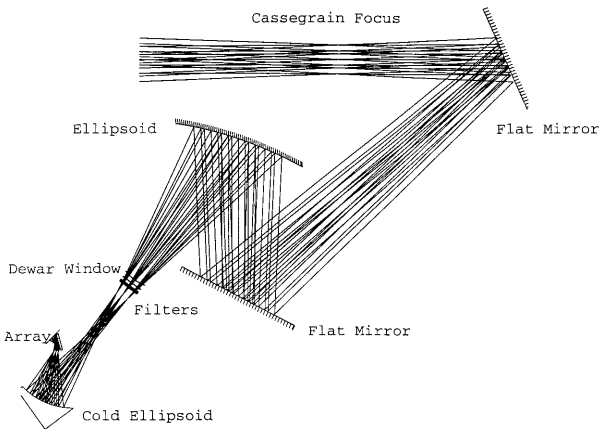

Fig. 2. Optics of the CSO bolometer camera.

age, the light rays pass through the cryostat's vacuum window, three infrared blocking filters (one cooled by the nitrogen shield and two by the helium shield), and a helium-cooled bandpass filter. An aperture stop, cooled by the ^{4}He bath, is mounted at the image of the primary mirror inside the cryostat. The focal plane formed by the relay optics is located below the aperture stop where a helium-cooled slit is located. The cold slit together with the cold aperture stop prevent unwanted light from reaching the detector and hence define the beam. The slit is reimaged by another off-axis, helium-cooled elliptical mirror onto the bolometer array. The light reflects off a flat mirror before reaching the pixels. The Dewar optics are described in more detail by Hunter *et al.*[5]

C. Optical Components

1. *Vacuum Window*

A sheet of 1-mm-thick high-density polyethylene is used as the vacuum window. We chose polyethylene so as to obtain small deflection under vacuum and good transmission in the 350- and 450-μm atmospheric windows. The vacuum window has a circular opening 6.4 cm in diameter. When the cryostat is evacuated, the center of the polyethylene window deflects into the Dewar by approximately 0.46 cm, which does not affect the optics significantly. We seal the polyethylene window to the Dewar with an o-ring, with no detectable helium leak or diffusion, at a level of 10^{-9} l atm/s. The transmission of the vacuum window in the 350- and 450-μm windows, measured with a Fourier transform spectrometer, is approximately 95%, which is consistent with results found in the literature.[6] Most of the loss is due to surface reflections. We considered the possibility of using a single-crystal quartz vacuum window, but the thickness required for such a large opening gives a lower transmission compared with polyethylene. We also considered using Mylar, but we were concerned about the possibility of gas diffusion through the Mylar sheet, large deflection over such a large aperture, as well as poor transmission for the required thickness.

2. *Infrared Blocking Filters*

Undesired radiation from visible wavelengths to approximately 170 μm is absorbed by a series of three infrared blocking filters,[5] which were purchased from Infrared Laboratories,[7] and have approximately 80% transmission for each filter in the passband. The first filter in the series is a 1.5-mm-thick, 5.71-cm-diameter single-crystal z-cut quartz wafer. It is antireflection coated at 400 μm with black polyethylene on both sides. This filter's function is to block radiation from visible wavelengths to approximately 50 μm. The filter is pressed against the lid of the nitrogen radiation shield with an aluminum ring, which makes contact with the filter at three points through three nearly fully compressed stainless-steel springs (Part No. C0088-012-0120M), applying a combined force of approximately 3 N (Ref. 8). Such a clamping mechanism allows for thermal contractions and ensures a good thermal contact between the filter and the shield lid. When the instrument operates with the vacuum window exposed to 300-K blackbody radiation, the filter temperature is approximately 95 K. This is determined mainly by the thermal conductivity of the nitrogen shield, which is 64 cm tall, 28 cm in diameter, and made of 0.13-cm-thick rolled aluminum.

Directly underneath the nitrogen quartz filter are two filters that are mounted on the lid of the helium radiation shield. The upper filter is a 2.5-mm-thick, 2.25-in (5.71-cm)-diameter, z-cut single-crystal quartz. It is antireflection coated at 400 μm on one side with clear polyethylene, and the other side has a diamond scatter layer. This filter is used to block radiation from the mid-infrared to approximately 100 μm. The lower filter is single-crystal CsI with the same dimensions as those of the helium quartz filter. The CsI filter is antireflection coated at 400 μm on both sides with clear polyethylene and is used to block radiation from 100 to approximately 170 μm. The clamping mechanism for both of these filters is the same as that for the nitrogen quartz filter. With these three blocking filters, we expect to reject all radiation from visible wavelengths to 170 μm. The rest of the undesired radiation is filtered by narrow bandpass filters.

3. *Bandpass Filters*

The submillimeter continuum camera is used to observe in the 350- and 450-μm atmospheric windows at the CSO. We purchased 350- and 450-μm resonant metal mesh bandpass filters with a clear aperture of 46 mm from Cochise Instruments, Inc.[9] These filters are made of layers of Mylar with a copper mesh pattern deposited on one side of each layer. They are designed to match the width of the atmospheric windows available from Mauna Kea (altitude, 4000 m), the site of the CSO.

The bandpass filters are installed so that they meet two conditions: (1) they operate at a temperature

close to the helium bath temperature and (2) they can be selected easily from outside the cryostat during observation. The filters are mounted on a filter wheel that is heat sunk to the helium bath. The mounting mechanism for these filters is the same as that used for the blocking filters. One selects a filter by turning a shaft from outside the cryostat. A counter is attached to the filter shaft to track the position of a filter. We can install four such filters on the filter wheel. Currently a 350- and a 450-μm bandpass filter are mounted on the wheel, and the other two positions are used to diagnose the system. The temperature of the filter wheel, when a filter is in position, is, at most, 0.1 K above the helium bath temperature. However, this does not guarantee that the Mylar layers, onto which the grids are deposited, are as cold as the filter wheel; we estimate the temperature of the grids to be no higher than 10 K.

4. Radiation Baffles

In addition to the aperture stop and the field stop, we installed radiation baffles to further eliminate light leaks. We achieved this by enclosing the aperture stop, the slit, and the cold off-axis elliptical mirror with a box, as shown in Fig. 1. The box is made of copper panels 0.025 in. (0.064 cm) thick, bolted to a rigid aluminum frame. The entire assembly is heat sunk to the helium bath. With such a configuration of light baffles, the only radiation coming from the vacuum window that can reach the bolometer array is that which passes through the aperture stop and the slit.

It is important to eliminate any radiation from 300-K parts or 130-K FET's. Because the photon energy is high from these sources, even when the photon flux is small, and exerts little excess power load on the bolometer, the fluctuation of such a flux can be large and hence dominate the NEP of the system. Therefore, in addition to our using an enclosed box, we found that it is necessary to baffle around the ^{3}He pot, where direct light could pass from the heat switches to the bolometer array, so as to prevent 300-K radiation from the heat switches from reaching the bolometer. Furthermore, we installed baffles around the filter wheel shaft and put the FET's in light-tight housings that were heat sunk to the ^{4}He bath.

To further reduce the scattered and reflected radiation from the surfaces of the baffling, the slit, the aperture stop, and the helium radiation shield, we painted them with Z306 aeroglaze (Lord Corporation[10]). We added to the paint, by volume, 3% carbon black and 11% solid-glass beads, with a mean diameter of 200 μm (Part No. A-glass 1922 and 2024) (Potters Industries, Inc.[11]). To make sure that the paint would stick well to the metal surfaces, we roughened the surfaces with grade 400 sandpaper and then rinsed the surfaces with methanol. A wash primer was required as an undercoat. The paint was sprayed on and was found to adhere well to both copper and aluminum surfaces and it also cycled well thermally.

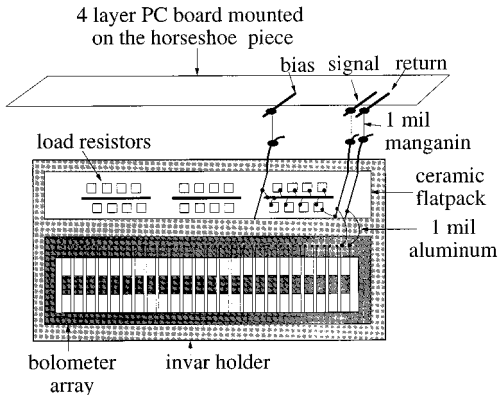

Fig. 3. Bolometer array layout.

3. Monolithic Bolometer Array

To optimize a bolometric instrument, it is necessary to understand the thermal and electrical properties of the bolometer. In this section we describe the structural parameters of the bolometer array, the electrical and thermal circuit, and the suspension of the array. We also present the results of the measurement of the array's electrical and thermal properties.

A. Structure

The bolometer array used in the submillimeter continuum camera (see Fig. 3) is a monolithic silicon array fabricated in the microelectronics laboratory at GSFC.[12] There are 24 pixels in the array, and the gap between adjacent pixels is approximately 15 μm. Each pixel is suspended by four long, thin silicon legs, which are formed by wet chemical etching; these thin legs provide a weak thermal link between the pixels and the heat sink, which is important so as to have a high sensitivity. The pixels are 1 mm × 2 mm × 12 μm, and the thin legs are 12 μm × 14 μm × 2 mm. The entire array is micromachined from a single silicon wafer.

Each pixel (see Fig. 4) consists of an absorber and a thermistor. The thermistor is deposited onto each pixel by phosphorus implantation with boron compensation; the doping has an appropriate density so that the thermistor's resistance at 300 mK is of the order of 10 MΩ. Electrical leads are implanted along two of the suspending silicon legs leading to the contact pads used for wire bonding.

Because silicon does not absorb submillimeter radiation, a bismuth film approximately 1100 Å thick is evaporated on the back of all the pixels, followed by 200 Å of SiO to protect the bismuth. We chose the bismuth thickness to optimize the pixel's absorptivity, which is at best 50%, by attempting to have an electrical impedance at the operating temperature that matches that of the free space.[13] Unfortunately, thickness is not the only parameter that determines the impedance of the bismuth film. Other factors, such as evaporation rate, the cleanliness of the evaporator, the temperature of the substrate during evaporation, etc., also have an effect on the electrical impedance. It is also possible that the film

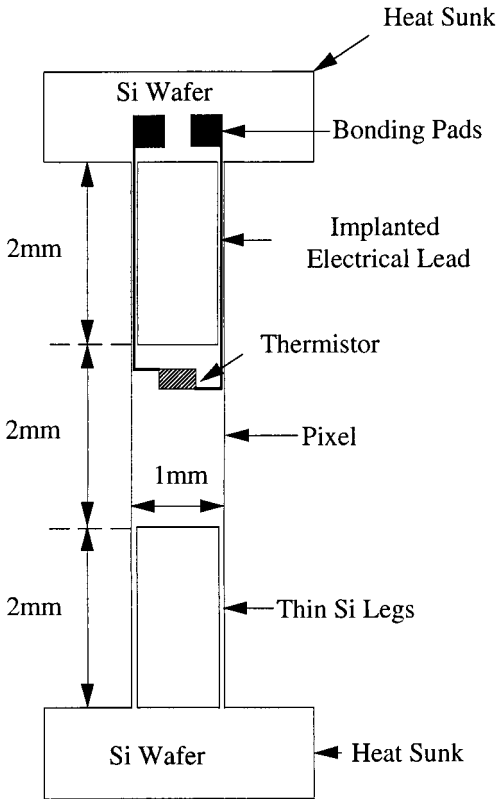

Fig. 4. Schematic drawing of a single pixel. The width of the thin silicon legs are exaggerated for this drawing.

impedance drifts over time. The impedance of the bismuth film on our array, measured at 4 K, gives an estimated absorptivity of approximately 35%, allowing some room for improvement.

B. Electrical Circuit

As in a conventional bolometer circuit,[14] the thermistor in each pixel is in series with a 30-MΩ metal film resistor, which is kept at the ^{3}He bath temperature on the same mount as the array. The combination is voltage biased. Signals from the thermistors are sent to cryogenically cooled FET's, which are connected as source followers. Signals from the FET's are then sent to the input of the room-temperature amplifiers (see Fig. 5).

C. Array Suspension and Thermal Isolation

The mechanical design of the instrument is important, as we must thermally isolate parts at different temperatures from one another, while keeping wiring lengths short and trying to avoid coupling mechanical vibrations to the signal wires and the thermistors.

The bolometer array is attached to an Invar holder with a single spot of glue at one point so as to avoid thermal stress. Invar is used because it has little thermal contraction from room temperature to cryogenic temperatures. All the load resistors are glued to a ceramic flatpack, which is glued to the Invar holder. The holder is cooled to the ^{3}He temperature by a copper finger. We made electrical connections

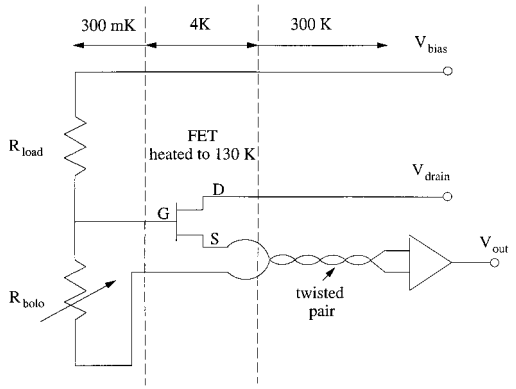

Fig. 5. Circuit diagram of a pixel.

between the thermistors and the load resistors by bonding ultrasonically 0.0025-cm-diameter aluminum wires between the contact pads on the array and the leads on the ceramic flatpack.

The Invar holder is suspended from an aluminum support shaped like a horseshoe with spring-loaded Kevlar threads; the support is mounted to the frame of the radiation baffle box (see Fig. 1) and is maintained at the helium bath temperature. Kevlar is a poor thermal conductor,[15] and therefore provides thermal isolation between the horseshoe piece and the Invar. The Kevlar threads are spring loaded to make the frequency of microphonic noise higher than that of signals, i.e., above 10 Hz.

The bias voltage for the load resistor–thermistor combination, and the signals from the pixels, are carried by a four-layer printed circuit (PC) board that is mounted on the horseshoe piece. Because the FET's are heated to 130 K and are plugged onto the PC board, great care must be taken to ensure that there is negligible heat flow from the FET's to the bolometers. The top and bottom layers of the board are ground planes that are used to heat sink the leads on the PC board, which is clamped to the horseshoe piece at several places to ensure a good thermal contact. We made the electrical connections between the Invar holder and the PC board by soldering 0.0025-cm-diameter and approximately 5-mm-long bare Manganin wires between them, maintaining the wires under tension. The wires are kept under tension so as to minimize any possible microphonic noise in the frequency range of interest. We used very thin Manganin wire to minimize the heat flow. We found that the ^{3}He bath temperature increases by only a few millidegrees Kelvin when the ^{4}He bath is at approximately 1.5 K and the FET's are heated to approximately 130 K. The pixel temperature, however, increases approximately 20 to 300 mK because the pixel has a weak heat link to the ^{3}He bath.

D. Electrical Properties: Resistance versus Temperature

To understand the performance of a bolometer, it is crucial to know the temperature dependence of the thermistor's resistance. Based on the doping level of our thermistors, we expect the resistance to be due to

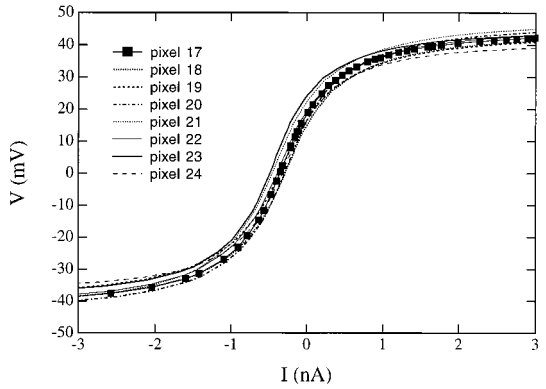

Fig. 6. I–V curves of eight pixels taken when the ^{3}He bath was at approximately 320 mK. Note the similar zero-bias resistance among all the pixels, indicating the uniformity of the array.

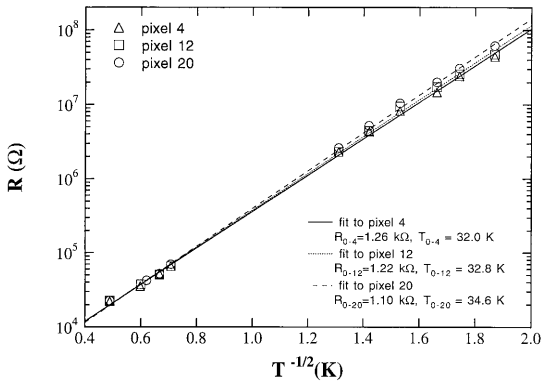

Fig. 7. Zero-bias resistance of three pixels as a function of temperature. The plot shows a good fit of the expected $R(T)$ to the data.

variable range hopping, giving rise to a zero-bias resistance of the form[16]

$$R(T) = R_0 \exp \sqrt{\frac{T_0}{T}}, \tag{1}$$

where $R(T)$ is the thermistor's resistance at temperature T, and R_0 and T_0 are constants specific to the thermistor.

We determined the zero-bias resistance by taking the current–voltage (I–V) characteristic of a pixel. We obtained an I–V curve by applying a bias voltage, supplied by a battery, to the bias resistor in series with the pixel and simultaneously recording the bias voltage and the voltage across the pixel with the data-acquisition system described in Section 5. In Fig. 6 we show some typical I–V curves of eight thermistor pixels taken simultaneously at a ^{3}He bath temperature of 298 mK. One can see from the data that the I–V curves of all eight pixels are similar, as are their zero-bias resistances. The shifts in the I–V's between different pixels indicate different thermoelectric voltages for each pixel. From the I–V's taken at different ^{3}He temperatures, one can obtain the zero-bias resistance as a function of temperature.

In Fig. 7 we show the measured zero-bias resistance at different temperatures for three pixels. We also show the corresponding fits to Eq. (1). From Fig. 7 one can see that Eq. (1) describes the temperature dependence of the zero-bias resistance rather well. The fact that three different pixels have a similar temperature dependence indicates that the pixels have similar electrical properties, an important feature required for an array used in a camera.

E. Thermal Properties: Thermal Conductance

In addition to the electrical behavior of a bolometer, it is important to understand its thermal conductance. In this section, we describe the measured thermal conductance of the bolometer $G(T)$ and compare it with the expected value.

One can obtain the thermal conductance of a bolometer from the I–V characteristic if one assumes that the bolometer resistance at any bias point $R = V/I$ gives the temperature of the bolometer according to the formula for the zero-bias resistance, i.e., $R = R_0 \exp(T/T_0)^{1/2}$. At any bias point (I, V), one can then calculate the temperature of the bolometer from

$$T = T_0 \left[\ln\left(\frac{R}{R_0}\right) \right]^{-2}, \tag{2}$$

where R_0 and T_0 are known from the measurement of the temperature dependence of the zero-bias resistance. An I–V curve can then be replotted in terms of bias power $P = IV$ as a function of the bolometer temperature, which then gives the thermal conductance of the bolometer as a function of temperature $G(T) = \mathrm{d}P/\mathrm{d}T$.

In Fig. 8 we show bias power P as a function of $T^4 - T_{\mathrm{sink}}{}^4$, where T_{sink} is the temperature of the heat sink (the ^{3}He bath temperature). The data show that P is proportional to $T^4 - T_{\mathrm{sink}}{}^4$, giving rise to a thermal conductance $G(T)$:

$$G(T) = \frac{\mathrm{d}P}{\mathrm{d}T} = 3.2 \times 10^{-8} T^3. \tag{3}$$

The T^3 temperature dependence is what we expect because the thermal conductance of the pixel is provided mostly by the four thin suspending silicon legs. Silicon is an insulator at these temperatures, and thus the thermal conduction is carried by phonons whose thermal conductance has a T^3 temperature dependence.

We also can estimate the value of the thermal conductance of the silicon legs with some simple expressions. We know that for a phonon gas, the thermal conductivity is given by

$$g = \tfrac{1}{3} c_v v l, \tag{4}$$

where g is the thermal conductivity, c_v is the specific heat, v is the speed of sound, and l is the mean free path of the phonons. From the Debye model, c_v is

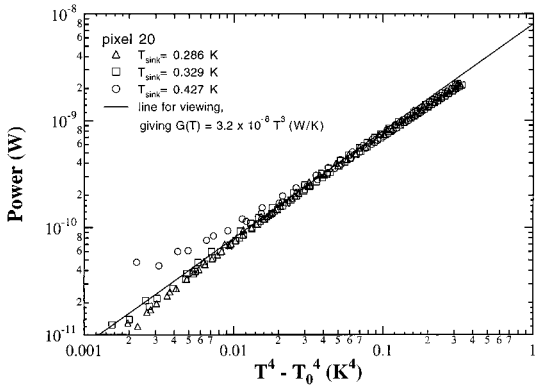

Fig. 8. Bias power as a function of temperature for pixel 20 at three ^{3}He pot temperatures. The solid line is a guide for viewing, not a fit. This figure shows that the data support a thermal conductance proportional to T^3.

given by

$$c_v(T) = 1944\left(\frac{T}{T_D}\right)^3 (\mathrm{J/K\ mol}), \quad (5)$$

where T is the temperature of the phonons, and T_D is the Debye temperature of the material under consideration. For silicon, $T_D = 700$ K, and $\upsilon = 5000$ m/s (for longitudinal phonons). We assume that the mean free path is limited by the smallest dimension of the silicon legs, $l = 12$ μm, although it may be several times this if the phonons can make specular bounces. From Eq. (4) and Eq. (5), we can estimate the thermal conductance $G(T)$:

$$G(T) = g(T) \times 4 \times \frac{A}{L} = 3.2 \times 10^{-9} T^3 (\mathrm{W/K}), \quad (6)$$

where A is the cross section of the silicon leg, and L is the length of the leg.

Comparing Eq. (6) with Eq. (3), we see that the estimated thermal conductance is approximately one tenth as large as the measured one, even though they have the same temperature dependence. This could be explained by the difference between the real mean free path, which is difficult to know, and that used in our estimate. Of course, there could be other factors that could cause this difference. On the other hand, it is quite good that one can obtain an order of magnitude estimate of $G(T)$ from such a simple model. Even though Fig. 8 shows the data from only one pixel, other pixels have very similar $G(T)$. The uniformity of $G(T)$ together with the uniformity of $R(T)$ for all the pixels implies that the pixels will have very uniform sensitivity.

4. Electronics

To build a sensitive bolometric instrument, one needs to properly design the system so that one can minimize microphonic noise as well as electrical cross talk between different channels. In addition, rf noise has to be blocked because it will heat up the bolometer and reduce its sensitivity. Finally, one has to ensure that electronic noise from the FET's and the amplifiers is low enough so that the instrument's sensitivity is background limited. In this section, we describe what we have done in these areas, and we show the measured noise spectrum of our FET's and amplifiers.

A. Microphonics

The major source of the microphonics comes from the pump on the ^{4}He bath. We operate the instrument while pumping on the bath so as to reduce the radiative and conductive heat loads on the bolometer from the shield and the array support. Because the signal frequency is mostly below 5 Hz, as we normally chop at 4 Hz, we need to make sure that little low-frequency vibration is coupled to the bolometer array from the pump. This is realized by a careful design of the suspension of the bolometer array and by proper wiring of the array. We made the suspension as stiff as possible by tensioning the Kevlar. We soldered all the wires to the array under tension. As a result, we saw no microphonic noise under 20 Hz, neither in the laboratory nor at the observatory.

B. Radio Frequency Noise

We have done two things to try to reduce the coupling of rf noise from the environment to the bolometer array. On all the signal lines going into the cryostat we installed rf filters with a cut-off frequency of approximately 1 MHz [electromagnetic interference filters (Part No. 56-726-005) from Spectrum Control, Inc.[17]] on the electrical feedthroughs on the cryostat. To eliminate digital noise from the computer that is used to process the data, fiber-optic cables are used to transmit all signals to the computer. The fact that the measured zero-bias resistance as a function of temperature gives the expected relation with no flattening at the low temperatures is a good indication that there is no significant amount of heating from rf noise. Any noticeable rf noise absorbed by a pixel will decrease its zero-bias resistance, especially at the lowest temperatures, and will make the data deviate from Eq. (1).

C. Electrical Cross Talk

To minimize electrical cross talk between different channels, each pixel has its own circuit ground, and the ground line is kept close to the signal line from the pixel to the input of the room-temperature amplifier. Twisted pairs made of 0.0125-cm-diameter Manganin wires are used inside the cryostat to connect from the FET's to the electrical feedthroughs on the cryostat. The grounds of all the pixels are connected together in the preamplifier. At the output of the amplifier, the signals with their separate grounds are connected to the differential inputs of the ADC's with a cable made of twisted pairs for which the ADC's have a shield for each pair. We found very little electrical cross talk between different pixels with this design.

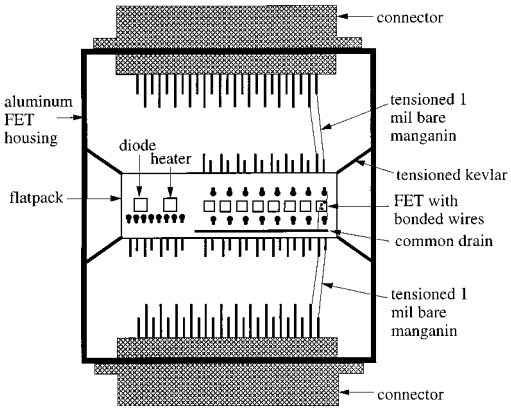

Fig. 9. Schematic drawing of the FET housing. It is not exactly a scaled drawing. The dimensions of the flatpack are 2 cm × 0.5 cm.

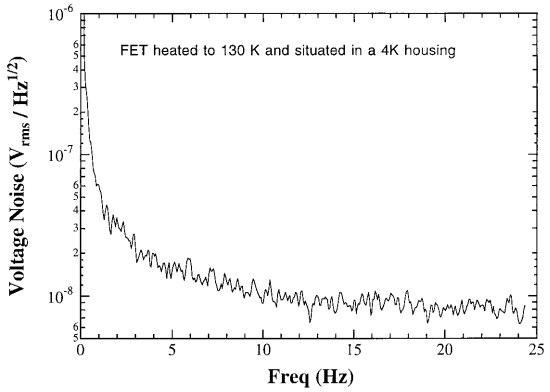

Fig. 10. Noise power spectrum of the electrical system recorded in the laboratory with a spectrum analyzer. The spectrum was taken when the gate of the FET was connected to a pixel cooled to 300 mK and biased at zero volts, the source of the FET was connected to the input of the room-temperature amplifier, and the FET was heated to approximately 130 K. The noise of the system at 4 Hz is approximately 20 nV/$\sqrt{\text{Hz}}$. Note that microphonic noise is absent in this spectrum.

D. Electrical Grounding

To avoid 60-Hz pickup, we designed the circuit ground with great care. The room-temperature amplifiers are powered by batteries. The ground of all the channels are kept independent and floating from the cryostat. The cryostat is electrically isolated from the telescope. The circuit ground for every pixel is defined at only one point, which we chose to be the ground of the power supply for the preamplifier. With this setup, we saw little 60-Hz pickup when the camera was operated at the telescope.

E. Field-Effect Transistors

FET's are used for the first stage of amplification as source followers to transform the high-pixel impedance into a low-source impedance. The FET's are the NJ14AL16 FET's from InterFET.[18] They are preselected, at room temperature, to have low noise, as well as to have I_{dss} (the drain-source current with gate shorted) less than 2 mA. Eight FET's are placed in a light-tight FET housing (see Fig. 9), which is mounted on the four-layer PC board.

Because these are silicon FET's, which do not work at 4 K, they are heated to approximately 130 K to obtain the lowest noise. Figure 9 shows a schematic of the FET housing, including the suspension of the package inside the housing. Eight FET's, all in their die form, are glued to a specially designed flatpack (Part No. SD560-9847) from Kyocera America, Inc.,[19] along with a heater and a diode thermometer. The FET's are wire bonded to the leads on the flatpack. A lid is glued to the flatpack to protect the FET's. The flatpack is suspended from its aluminum housing with Kevlar threads kept under tension by compressed springs. The Kevlar suspension allows us to establish a temperature gradient between the flatpack at approximately 130 K (when the FET's are heated) and the housing, which is heat sunk to the ^{4}He bath. Bare Manganin wires 0.0025 cm in diameter and approximately 5 mm long are soldered under tension between the flatpack and the connectors on the FET housing. We used small wires to keep the heat conduction from the FET's to the PC board to a minimum. Again, the wires are under tension to keep the microphonics at high frequencies. With the care we have taken, we find that the temperature increase of the four-layer PC board that is due to the heat from the FET's when they are heated to 130 K is only approximately 0.2 K, which does not affect noticeably the pixel impedance.

Figure 10 shows the total noise power spectrum of a typical channel. The spectrum was recorded when the gate of the FET was connected to a pixel looking at a 4K blankoff, biased at zero voltage and cooled to approximately 300 mK, the source of the FET was connected to the room-temperature amplifier, and the FET was heated to approximately 130 K. The expected Johnson noise from the 30-MΩ load resistor and the zero-bias resistance of the pixel, which is approximately 30 MΩ, is approximately 16 nV/$\sqrt{\text{Hz}}$. The measured noise of the room-temperature amplifier at 4 Hz is approximately 10 nV/$\sqrt{\text{Hz}}$. Figure 10 suggests that the noise from the FET itself is approximately 10 nV/$\sqrt{\text{Hz}}$ at 4 Hz. We note that there is no significant microphonic noise present in Fig. 10, even though the ^{4}He bath was pumped by a mechanical pump when the noise spectrum was recorded.

5. Data-Acquisition System

We built our own ADC's for the array with a design by R. Baker and colleagues at GSFC. Lock-in detection is performed with a specially designed DSP board residing inside a Macintosh computer. Data-acquisition software is written in Labview on the Macintosh, which is linked to the telescope control computer by way of Ethernet.

A. Analog-to-Digital Converters

In Fig. 11 we show the flow chart of the data-acquisition hardware. The differential signals from the output of the room-temperature amplifiers are fed to the differential inputs of the 16-bit ADC's,

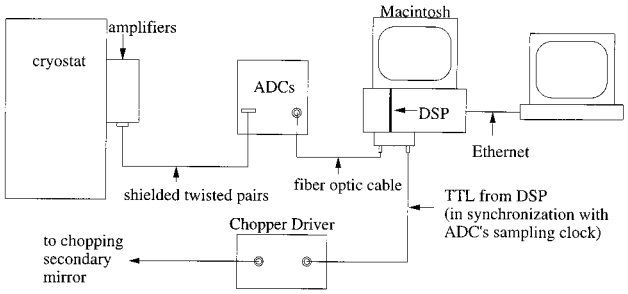

Fig. 11. Diagram of the data system for the camera.

which have an input range of −3 to 3 V and a sampling frequency of 1 kHz, but can be increased to 40 kHz. Each channel has its own ADC chip, therefore signals from all the pixels are digitized simultaneously. The output of the ADC's are sent to the input of the DSP board with fiber-optic cables that are designed to isolate electrically the Macintosh computer from the instrument.

B. Digital Signal Processing Board

The DSP board uses the TM320C50 DSP chip from Texas Instruments. To synchronize the lock-in detection with the chopping secondary, a transistor–transistor logic (TTL) signal, generated by the DSP board, is used to produce the signal that drives the chopping secondary mirror. The chopping frequency can be set to 1 kHz/n, where 1 kHz is the ADC sampling frequency and n is an integer between 1 and 1024. The chopping frequency defined in this way is synchronous with the ADC sampling frequency. The ADC, therefore, samples the signal starting at the same place for every chop cycle.

6. Characteristics of the Camera

When constructing an instrument for a ground-based telescope, one's aim is to have the instrument's sensitivity limited by the fluctuation of the background radiation from the sky. For a bolometric instrument, this means that the bolometer's responsivity needs to be high and that the system's noise needs to be low.

If we assume that the NEP from the fluctuation of the background radiation is $\mathrm{NEP}_{\mathrm{bkgd}}$ (W/$\sqrt{\mathrm{Hz}}$), the optical responsivity of the instrument is $\Re$ (V/W), and the voltage noise of the entire system is e_n (V/$\sqrt{\mathrm{Hz}}$), then the NEP of the instrument is

$$\mathrm{NEP} = \frac{e_n}{\Re}. \tag{7}$$

For the instrument to be background limited, the instrument's optical responsivity needs to satisfy

$$\Re \gg \frac{e_n}{\mathrm{NEP}_{\mathrm{bkgd}}}. \tag{8}$$

In this section, we present the expected background noise, describe the measured optical responsivity, and deduce the optical NEP for the camera.

A. Background Noise

The background noise comes from the fluctuations of the sky's blackbody radiation at approximately 280 K. The NEP, referred to the entrance of the cryostat, can be estimated by[20,21]

$$\mathrm{NEP}_{\mathrm{bkgd}} = \left[\frac{4\varepsilon h\upsilon k_B T_B \Delta\upsilon}{\eta}\left(1 + \varepsilon\eta\,\frac{k_B T_B}{h\upsilon}\right)\right]^{1/2}, \tag{9}$$

where ε is the emissivity of the sky, h is Planck's constant, υ is the radiation frequency, k_B is Boltzmann's constant, T_B is the temperature of the background radiation, $\Delta\upsilon$ is the bandwidth of the bandpass filter, and η is the total quantum efficiency of the system. For a reasonable night with $\varepsilon = 0.5$, $T_B = 280$ K, and a quantum efficiency of 10%, we find $\mathrm{NEP}_{\mathrm{bkgd}} \approx 2 \times 10^{-15}$ W/$\sqrt{\mathrm{Hz}}$ at 450 μm for a bandwidth of 100 GHz.

B. Optical Responsivity

We measured the optical responsivity of the camera in the laboratory. A room-temperature elliptical mirror is mounted on the bottom of the cryostat to reimage the slit inside the cryostat onto an external chopper wheel. The chopper wheel chops at 10 Hz between 300- and 77-K sources. For our 450-μm bandpass filter, we expect 320 pW on each pixel for 300-K radiation and 80 pW for 77 K, estimated with the expression of $2k_BT \times (A\Omega/\lambda^2) \times \Delta\upsilon$, where A is the area of the pixel, Ω is the solid angle that the pixel subtends to the aperture stop, λ is the wavelength, and $\Delta\upsilon$ is the bandwidth of the bandpass filter, which is approximately 100 GHz for both the 350- and the 450-μm filters. At 450 μm, the signal observed on all the pixels is approximately 2.2 mV peak to peak, resulting in an optical responsivity of 9×10^6 V/W. Similarly, for the 350-μm filter, the input power at the vacuum window is approximately 400 pW, and the peak-to-peak signal is approximately 4.6 mV, which give an optical responsivity of 1×10^7.

C. Total Quantum Efficiency of the Camera

We measured the total quantum efficiency of the camera. We record the pixels' I–V curves when we expose the polyethylene window to 300- and 77-K radiation. From the zero-bias resistance, one can obtain the temperature of the pixel. With the thermal conductance $G(T)$ measured earlier, one can estimate the power absorbed by the pixel:

$$P = \int_{T_{\mathrm{sink}}}^{T_{\mathrm{bolo}}} G(T)\mathrm{d}T. \tag{10}$$

The power absorbed by each pixel with the 450-μm filter in place is estimated to be 34 pW when the bolometers are exposed to 300-K radiation and 13 pW when they are exposed to 77-K radiation. Because of excess power on the pixel from surrounding walls and some possible small light leaks, the quantum efficiency is estimated with the ratio of the power difference between 300- and 77-K radiation. This

gives a total quantum efficiency in the 450-μm window of approximately 9%. Similarly, the total quantum efficiency in the 350-μm window is approximately 10%. Note that both the quantum efficiency and the optical responsivity at 350 μm are slightly better than those at 450 μm. This is primarily because diffraction is less important at 350 μm.

From the measured impedance of the bismuth film at 4 K, we anticipate a 30% absorptivity for the pixels alone. The polyethylene window is expected to transmit approximately 90%, as is the 450-μm bandpass filter. The infrared blocking filters at 77 and 4 K are expected to have a transmission of approximately 80% in the passband. The product of all these transmissions gives an estimated total quantum efficiency of approximately 12%. If we assume that the emissivity of the sources is approximately 90%, then the expected quantum efficiency is approximately 11%. The measured value of 9 to 10% is therefore reasonable.

D. Noise-Equivalent Power of the Camera

A proper NEP measurement calls for the noise measurement when the camera looks at a blank piece of sky, as well as the responsivity measurement under the same situation. We measured the camera's noise on the telescope when the camera was staring at a blank piece of sky. However, we did not perform the responsivity measurement in the same way. Because the effective temperature of the sky is approximately 150 K, assuming a 50% emissivity, and most of the sources are at a temperature near that of the sky, the responsivity of the camera on a source likely will be a little different from that described in Subsection 6.B. As a result, the NEP described in this subsection is slightly different from the NEP on the sky. Nevertheless, it is a good indication of the camera's sensitivity.

We measured the noise of one pixel with a spectrum analyzer when the atmospheric opacity, τ, was 0.03 at 225 GHz and the telescope was staring at a blank piece of sky at a zenith angle of approximately 45°. The noise at 4 Hz was approximately 50 nV/$\sqrt{\text{Hz}}$, which gives

$$\text{NEP} = \frac{e_n}{\Re} \approx \frac{50 \times 10^{-9}}{1 \times 10^{7}} = 5 \times 10^{-15}\ \text{W}/\sqrt{\text{Hz}}. \quad (11)$$

This is approximately 2.5 times higher than the expected background noise. So the camera is not yet background limited.

With the measured optical responsivity of 1×10^7 and a background NEP of 2×10^{-15} W/$\sqrt{\text{Hz}}$, one needs to achieve a voltage noise less than 20 nV/$\sqrt{\text{Hz}}$ so as to be background limited. One can see from Fig. 10 that the voltage noise of the system is approximately 20 nV/$\sqrt{\text{Hz}}$ when the bias is grounded. As soon as we apply a bias voltage, the noise increases to approximately 50 nV/$\sqrt{\text{Hz}}$. Because this excess noise is present only when the bias is on, it is probably caused by a light leak. Given that we did a careful baffling job around the light entrance to the Dewar and around the ^{3}He pot, we suspect that the possible place for this leak comes from the heated FET's. We are in the process of eliminating this excess noise and making the camera background limited.

E. Noise-Equivalent Flux Density of the Camera and Telescope System

We made an independent measurement of the NEFD above the atmosphere, at 350 μm, from observations of Uranus at an airmass of 1.33. The average optical depth across the camera filter measured directly from the dependence of the observed intensity of Saturn as a function of the airmass was 0.6. At the time when the data were taken, approximately 50% of the noise in the map was correlated among all the pixels. This correlated component can be removed, though not completely, in data-reduction software. The remaining uncorrelated noise component gives a NEFD of approximately 4–9 Jy/$\sqrt{\text{Hz}}$ over different parts of the map. Since then we have eliminated the source of the correlated noise, and the rms noise has improved by at least a factor of 2. Unfortunately Uranus was unavailable for a recalibration. Based on the signal-to-noise ratio (SNR) on known sources, we estimate the camera's NEFD to be approximately 4 Jy/$\sqrt{\text{Hz}}$ under good weather conditions.

The NEFD measurement is consistent with the NEP measurement described above. We know that the primary mirror has an area of approximately 80 m^2 and that the 350-μm bandpass filter has a bandwidth of 100 GHz. To compute the NEFD from the NEP, we need to take into account the transmission of atmosphere, the main beam efficiency, the fact that Uranus is a point source and the pixel size is smaller than the diffraction-limited beam size, and that background radiation is extended. If we assume that the main beam efficiency at 350 μm is approximately 30% (as deduced by application of the Ruze formula to lower-frequency measurements made with the heterodyne instruments), the atmosphere has a transmission of 30%, and that only 35% of the diffraction beam flux from Uranus entering the cryostat reaches a given pixel, a NEP of 5×10^{-15} W/$\sqrt{\text{Hz}}$ is equivalent to a NEFD of 2.3 Jy/$\sqrt{\text{Hz}}$.

F. Calibration of all the Pixels

We checked the relative sensitivity of all the pixels by pointing each pixel at Saturn and recording the signal from all the pixels. The SNR from a pixel when Saturn is pointed at that pixel is a good measure of the corresponding sensitivity. Figure 12(a) shows the SNR of all the pixels from four different scans. One can see that the SNR varies approximately a factor of 2 from pixel to pixel. For the observation of astronomical sources, it is also important to know the relative gain of all the pixels, which is well characterized by the peak value from each pixel when Saturn is pointed to that pixel. In Fig. 12(b) we show the peak value from each pixel from the four different scans. We note that the variation on the gain among

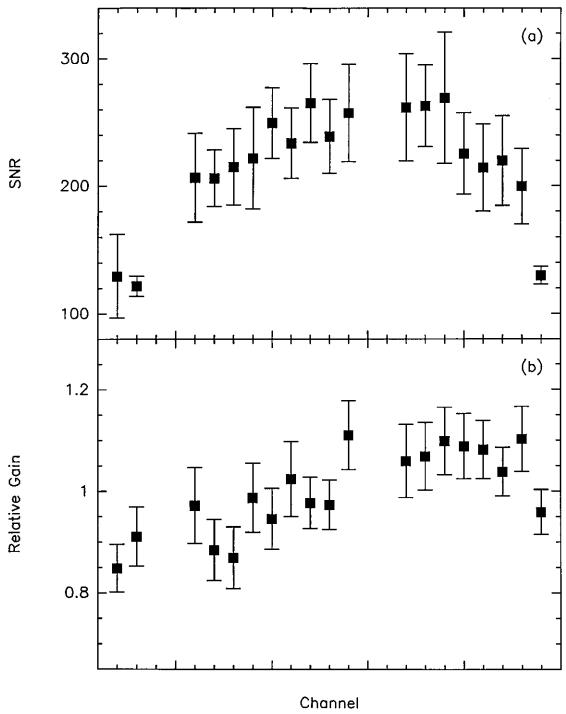

Fig. 12. (a) Signal-to-noise ratio of all the pixels when each pixel was pointed at Saturn. The filled square is the mean of four scans, and the error bar indicates the rms. (b) Relative gain of all the pixels. The gain is taken as the peak value from each pixel when it is pointed at Saturn. The filled square is the mean of the four scans, and the error bar is the rms. Note that pixels 1, 5, 15, and 16 are not functional.

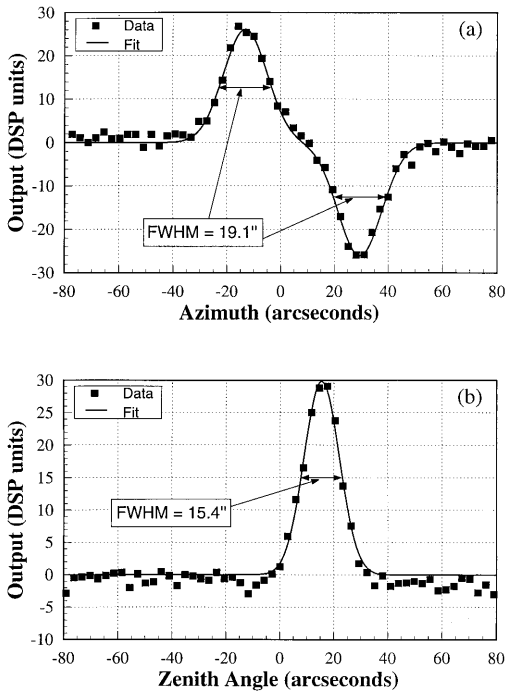

Fig. 13. Lock-in signal from one pixel as it scanned across Saturn in azimuth and zenith angles at 350 μm. The data were taken in October 1995 when τ (225 GHz) was approximately 0.075, the chopping frequency was 4 Hz, and the chop throw was 43 arc sec. The integration time per point was 0.976 s, although for the azimuth scan the data were taken at 0.244-s intervals and binned. The apparent size of Saturn during the time the data were taken was 18.8 arcsec × 16.8 arcsec. (a) The azimuth scan data are fit by a mirrored Gaussian profile in which the azimuth offset, the amplitude, the FWHM, and the separation are the four free parameters. (b) The zenith angle scan data are fit by a single Gaussian, in which the free parameters are the amplitude, the FWHM, and the zenith angle offset.

all the pixels is approximately 30%, much smaller than that of the SNR. This shows that the noise varies more from pixel to pixel. Further studies are needed to understand this difference.

G. Light Leaks

In a design that does not use Winston cones, it is crucial to eliminate all the light leaks with baffles. We enclosed the ellipsoid with a metal box cooled to the ^{4}He bath temperature, as shown in Fig. 1. The interior of this metal box is painted black so as to absorb any radiation that reaches it. Any small gap between the array holder and the metal box is covered with aluminum tape to prevent radiation from reaching the pixels. The ^{3}He pot is completely baffled, except for a small opening for a cold finger to be connected to the Invar holder to reduce any possible light leak from the heat-switch activation mechanism. The FET's, which are at approximately 130 K during normal operation, are kept inside a light-tight aluminum housing heat sunk to the ^{4}He bath. With these efforts, we found that the light leak through the vacuum window is approximately 0.1% of the 350-μm signal size. However, there might still be some light leak that is due to the warm FET's, which could explain the excess noise seen with the bias on. We are in the process of understanding and trying to eliminate this light leak.

H. Optical Performance

We checked the optics of the camera on the telescope. We were able to use Saturn to check the pointing and the focus, the results of which came out to be reasonable. To check the alignment between the optical components we scanned over Saturn both in azimuth and in zenith angle and plotted the digital lock-in result from the DSP in Fig. 13. The FWHM in both directions coincides well with the size of Saturn, convolved with the telescope Airy pattern and by our taking into account the finite size of the pixel, to within 1 arc sec, indicating that the camera is diffraction limited, as expected.[5] There are no noticeable bumps on the tail end of the peak, which demonstrates that the alignment between all the optical components is very good. Because each pixel subtends 5 arc sec × 10 arc sec on the sky, and the diffraction-limited beam size is approximately 10 arc sec at 400 μm, we therefore have Nyquist sampling along the length of the array at 350 and 450 μm, as the gap between two adjacent pixels is only 15 μm.

We also made an on-the-fly map of the molecular cloud NGC 2024 at 350 μm shown in Fig. 14. We scanned all the pixels across the source, and Fig. 14

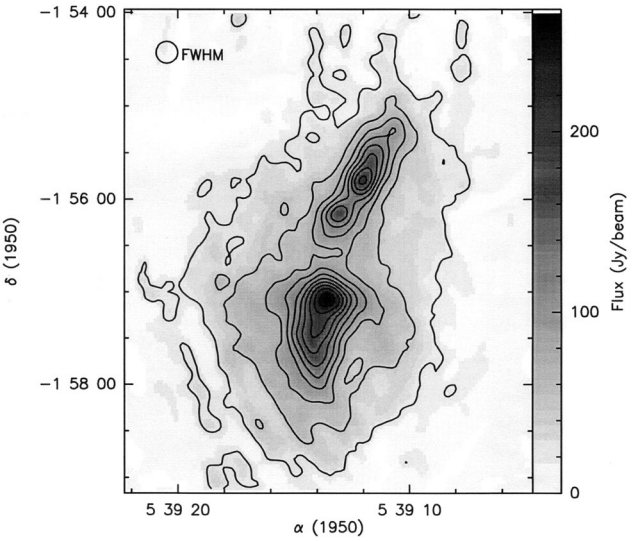

Fig. 14. Gray-scale image of the 350-μm continuum emission toward NGC 2024, a star-forming region located in the Orion Molecular Cloud. The data were taken in October 1995 when we scanned the camera at a constant elevation when $\tau = 0.05$ at 225 GHz with a chopping frequency of 4 Hz and a chop throw of 48 arcsec. The resulting dual-beam scans were restored with the NOD-2 algorithm and then interpolated onto regular grid in the equatorial coordinate system. The effective angular resolution is approximately 14 arc sec, and the contour levels are 25–250 Jy/beam in intervals of 25 Jy/beam. The rms noise level is approximately 5.5 Jy/beam. The absolute calibration uncertainty is approximately 30%.

is the σ-weighted average of the data from all the pixels. The data were taken with $\tau = 0.05$ at 225 GHz, an air mass of 1.1 to 1.2, a chopping frequency of 4 Hz, and a chop throw of 48 arc sec.

7. Conclusion

In summary, we constructed a submillimeter continuum camera operating at the 350- and 450-μm atmospheric windows. It has an optical responsivity of approximately 1×10^7 V/W, a total quantum efficiency of approximately 10%, an optical NEP of approximately 5×10^{-15} W/$\sqrt{\text{Hz}}$, and a NEFD of approximately 4 Jy/$\sqrt{\text{Hz}}$ for τ_{225} of 0.03 and an air mass of 1.33. We have Nyquist sampling along the 24 pixels. However, the camera has not yet reached its optimal sensitivity as there still exist some excess noise related to bias. We are in the process of trying to eliminate this excess noise to make the camera background limited.

We thank the people in the microelectronics lab at the GSFC for fabricating the array, R. Kelley for the FET's, S. Murphy for many helpful discussions on FET suspension, J. Keene for discussions on filters, and B. Smith for wiring the circuit boards. We thank A. Cleland for helping out with many tests in the laboratory and for many discussions on bolometer physics. D. Vail has made many of the important parts on the cryostat, and people at the central engineering and physics shops at Caltech helped out with many rush jobs. We are grateful for all the help from the CSO staff, in particular, A. Schinckel, K. Young, A. Guyer, and M. Houde. We also thank W. Schaal for help with mechanical designs. This work was supported by National Science Foundation grant AST-9313929. D. J. Benford is supported by a NASA graduate student research fellowship.

References and Notes

1. D. A. Harper, R. H. Hilderbrand, R. Stiening, and R. Winston, "Heat trap: an optimized far infrared field system," Appl. Opt. **15,** 53–60 (1976).
2. The cryostat is made by R. Pernick at Yerkes Observatory, 373 West Geneva St., Williams Bay, Wisc. 53191.
3. E. Serabyn, "Wide-field imaging optics for submm arrays," in *Multifeed Systems for Radio Telescopes*, ASP Conference Series, Vol. 75, E. T. Emerson and J. M. Payne, eds. (Astronomical Society of the Pacific, San Francisco, Calif., 1995), pp. 74–81.
4. E. Serabyn, "A wide-field relay optics system for the Caltech Submillimeter Observatory," Int. J. Infrared Millimeter Waves (1996).
5. T. R. Hunter and E. Sarabyn, "Optical design of the submillimeter high angular resolution camera (SHARC)," Publ. Astron. Soc. Pac. (1996).
6. G. W. Chantry, J. W. Fleming, and P. M. Smith, "Far infrared and millimeter-wave absorption spectra of some low-loss polymers," Chem. Phys. Lett. **10,** 473–477 (1971).
7. Infrared Laboratories, 1808 East 17th St., Tucson, Ariz. 85719 (personal communication, 1995).
8. Associated Springs, P.O. Box 3296, Cerritos, Calif. 90703 (personal communication, 1995).
9. Cochise Instruments, Inc., 6304 deMello St., Hereford, Ariz. 85615 (personal communication, 1995).
10. Lord Corporation Industrial Coatings, 2000 West Grandview Blvd., P.O. Box 10038, Erie, Penn. 16514-0038 (personal communication, 1995).
11. Potters Industries, Inc., Waterview Corporate Centre, 20 Waterview Blvd., Parsippany, N.J. 07054-1282 (personal communication, 1995).
12. S. H. Moseley, J. C. Mather, and D. J. McCammon, "Thermal detectors as x-ray spectrometers," J. Appl. Phys. **56**(5), 1257–1262 (1984).
13. J. Clarke, G. I. Hoffer, P. L. Richards, and N.-H. Yeh, "Superconductive bolometers for submillimeter wavelengths," J. Appl. Phys. **48**(12), 4865–4879 (1978).
14. R. C. Jones, "The general theory of bolometer performance," J. Opt. Soc. Am. **43,** 1–14 (1953).
15. J. G. Hust, "Low-temperature thermal conductivity of two fibre-epoxy composites," Cryogenics **15,** 126–128 (1975).
16. A. L. Efros and B. I. Shklovskii, *Electronic Properties of the Doped Semiconductors* (Springer-Verlag, New York, 1984).
17. Spectrum Control, Inc., 6000 West Ridge Rd., Erie, Pa. 16506 (personal communication, 1993).
18. interFET, 1000 N. Shiloh Rd., Garland, Tex. 75042 (personal communication, 1995).
19. Kyocera America, Inc., 95 Argonaut, Suite 190, Aliso Viejo, Calif. 92656 designed by Goddard Flight Space Center (personal communication, 1993).
20. T. G. Phillips, "Techniques of submillimeter astronomy," in *Millimeter and Submillimeter Astronomy*, R. D. Wolstencroft and W. B. Burton, eds. (Kluwer Academic, Boston, Mass., 1988), pp. 1–25.
21. N. Wang, T. R. Hunter, D. J. Benford, E. Serabyn, T. G. Phillips, and S. H. Moseley, "A monolithic Si bolometer array for the Caltech Submillimeter Observatory," in *Instrumentation in Astronomy VIII*, D. L. Crawford and E. R. Craine, eds., Proc. SPIE **2198,** 749–756 (1994).